Research Square

Preprints are preliminary reports that have not undergone peer review.
They should not be considered conclusive, used to inform clinical practice,
or referenced by the media as validated information.

Deformable image registration (DIRART) of targets and critical organs in prostate CBCT-guided adaptive radiotherapy: geometric and dosimetric evaluation

Hussam Hameed Jassim

husjas.iraq85@gmail.com

The University of AlKafeel

nooshin Banaee

Medical Radiation Research Center, Central Tehran Branch, Islamic Azad University, Tehran 1469669191, Iran.

Hassan Ali Nedaie

Radiation Oncology Research Centre, Cancer Institute, Tehran University of Medical Sciences, Tehran 1417613151, Iran

Toshikazu Imae

University of Tokyo Hospital

Short Report

Keywords: CBCT, deformable image registration, Radiotherapy

Posted Date: March 9th, 2026

DOI: https://doi.org/10.21203/rs.3.rs-9050573/v1

License: This work is licensed under a Creative Commons Attribution 4.0 International License.
Read Full License

Additional Declarations: The authors declare no competing interests.

Deformable image registration (DIRART) of targets and critical organs in prostate CBCT-guided adaptive radiotherapy: geometric and dosimetric evaluation

Hussam H Jassim[1], Hassan Ali Nedaei[1,3,*], Nooshin Banaee[2], Toshikazu Imae[5]

[1]Radiotherapy and Radiology Department, Middle Euphrates Cancer Centre, Kufa, Iraq

[2]Radiology Technology Department, Faculty of medical and health techniques, University of Al-Kafeel, Iraq

[3]Radiation Oncology Research Centre, Cancer Institute, Tehran University of Medical Sciences, Tehran 1417613151, Iran

[4]Medical Radiation Research Center, Central Tehran Branch, Islamic Azad University, Tehran 1469669191, Iran.

[5]University of Tokyo Hospital, Tokyo, Japan.

*Corresponding author: Hussam Hameed Jassim

Email: husjas.iraq@gmail.com

Abstract

Objectives: To evaluate different deformable image registrations (DIRs) for cone beam computed tomography (CBCT)-based dose calculations.

Methods: The registration accuracy were evaluated using CIRS phantom and five patients. Deformable planning computed tomography (pCT) and CBCT images registration of prostate cancer cases were conducted using 14 default registration methods and Anatomically Constrained Deformation Algorithm (ANACONDA) registration methods. Quantitative indices of image quality were uniformity, contrast-to-noise ratio, and signal-to-noise ratio for the phantom, and structural similarity index measure, mean absolute error, and peak signal to noise ratio (PSNR) for the patients. Registration accuracy was evaluated using Target Registration Error (TRE) and the Dice Similarity Coefficient (DSC).

Results: Compared to CBCT, dCT demonstrated considerably improved uniformity 75%, 65%, 77%, contrast-to-noise ratio 214%, 213%, 215%, and signal-to-noise ratio of 108%, 107%, 107% relative to those of CBCT in phantoms with iterative optical flow, B-spline, and ANACONDA registration methods, and improved structural similarity index measures by 14%, 9%, 9%, 11%, 21% and 14%, PSNRs 98%, 87%, 87%, 76%, 94%, and mean absolute errors 98%, 87%, 87%, 76%, 97%, 93% in patients for the Iterative Optical Flow (IOF), B-Spline, Systematic Force Demons (SFD), double force demons (DFD), free form (FF) and ANACONDA registration methods, respectively. Whereas the ANACONDA registration methods improved registration accuracy, within 0.2 cm TRE of prostate landmarks and by more than 90% DSC of critical organs, both IOF and B-Spline algorithms failed to reproduce the geometry for patients.

Conclusion: Therefore, ANACONDA registration has the potential to contribute to the improvement of adaptive radiotherapy.

Keywords: CBCT, deformable image registration, Radiotherapy

Introduction

Over the last two decades, radiation therapy has improved significantly via the incorporation of three-dimensional anatomy into planning systems, the development of intensity-modulated radiation therapy and image-guided radiation therapy techniques that allow for the individualisation of treatment [1-3]. Compared with three-dimensional conformal radiotherapy, these advancements in technology have improved dose coverage to the prostate without compromising radiation exposure to the surrounding normal tissues [4-5]. These developments have led to maximising tumour coverage and dose and/or generating a steep dose gradient with simultaneous reduction of toxicity, which has translated to an increase in the therapeutic index [6-7].

Image guided radiation therapy including the cone beam computed tomographyCBCT) images of patients are acquired daily using a Linac, Halcyon or Ethos unit for adaptive radiation therapy as well as online imaging verification [8]. CBCT images besides immobilization devices, and planning structures are mainly used for setting up reproducibility and managing internal organ deformation caused by normal physiological processes such as tumor shrinkage, and cavity filling [4, 9-10]. CBCT images can also be used to calculate the daily doses in many regions of the body, adjust the dose map to take into account the patient's accumulated dose, and auto-contour regions of interestROIs) [5, 11-13]. To accurately calculate the dose for CBCT prostate cancer patients, two features should be ensured:1) that the intensity values on CBCT are the same as those on planning computed tomographypCT), and2) that the geometry of the pelvis structures is the same as that on CBCT. However, CBCT images without correction are associated with an inaccurate HU that propagates into the dose distribution due to many reasons such as a large amount of scatter owing to the type of filter and collimator and acquisition parameters. [4, 14-15]. Furthermore, setup errors and internal organ motion are accounted for by using expansion margins to the clinical target volume, but these margins also increase dose to healthy tissues. These issues can be resolved by using deformable imaging registrationDIR) [16].

Many studies demonstrated that intensity-based, B-Spline and DIR with histogram matching or multilevel threshold image registrations can map the image intensity of pCT

voxel-to-voxel on CBCT images with acceptable results. Thus, the effects of Hounsfield unitHU) discrepancies between pCT and deformed CTdCT) on dose distribution using deformable vector fieldDVF) have negligible impact on dose distribution [13, 17-18]. Although Woerner et al. and Varadhan et al. stated that the use of B-Spline can propagate a contour from moving CT to a target CT of the same modality with acceptable accuracy, Shah e al.2021) argued that B-Spline algorithm fails in terms of accuracy in pelvic region when propagating a contour from moving CT to a target CT of the different modalitypCT to CBCT) [17, 19-21]. Issues that worsen registration accuracy are poor imaging quality, inconsistent visual features, intensity mismatching, differences in bladder filling status, and inconsistent visual features, remain [11, 17-18, 22-27]. Although they reported good dosimetric agreement, but they did not consider the atypical anatomy encountered in the clinic. Therefore, for ART to be reliable and effective, an accurate DIR-propagated scan must be generated; therefore, the accuracy of the available DIR algorithms must be validated before being applied clinically.

Currently, no study has considered the effects of both HU discrepancies and anatomical changes over the course of a treatment with intensity-based image registration and B-Spline image registration algorithms on dose distribution. Therefore, in this study, these two aspects were investigated using the default point-based method B-Spline algorithm) and intensity-based consistent image registration algorithms for intra-subject registration of the pelvis.

Methodology

Data of CT/ CBCT images

This study was divided into two parts. First, a CIRS phantom was used to evaluate the clinical applications of potential HU discrepancies between the Hounsfield electron density (HU-ED) calibration of the pCT and dCT images. A CIRS disc phantom containing nine plugs surrounded by a ring phantom containing eight plugs of different electron densities was used in this study [28]. Second, 11 patients with prostate cancer were recruited to evaluate the capacity of DIR-based techniques in managing atypical anatomy as recommended by TG-132 [29]. Several anatomical differences were taken into consideration, such as differences in bladder and rectal filling, as well as different positions of the femoral heads. In our analysis, patients with anatomical features that

differ from those seen on CBCT images were selected based on visual check of three authorsH.H.J, H.A.N and N.B) using checkerboard images of visualization options in the DIR software. CBCT and CT were used to contour target and organs-at-risk, and their volumes were compared. We included CT images of patient datasets with a volume difference below 95%) in our studies Fig.1. Thus, only five out of eleven patients were studied.

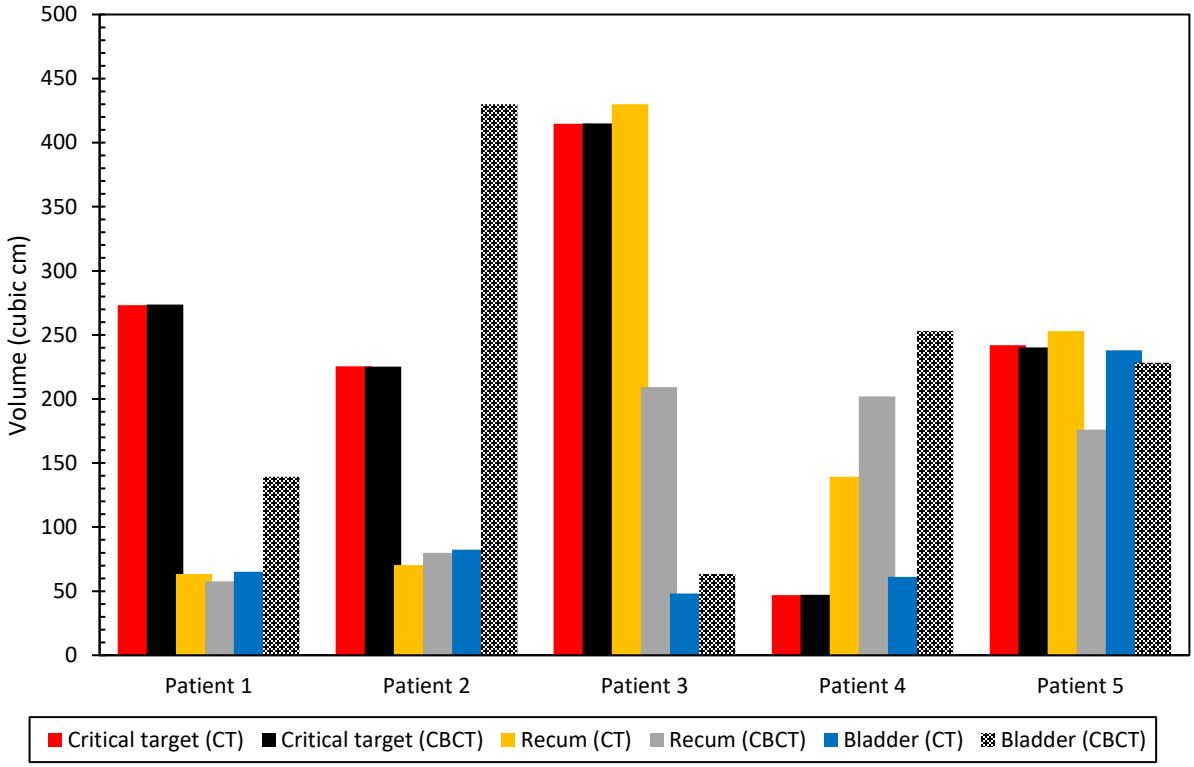


FIG.1. Comparing volumes of critical targets and organs-at-riskbladder and rectum) using pCT and CBCT for five patients. Legend: CT: Computed Tomography and CBCT: Cone Beam Computed Tomography.

All cases were independently scanned using CT, followed immediately by CBCT. The properties of the CT/ CBCT data are documented in Table 1.

TABLE 1. CT and CBCT data of the phantom and patients.

Electron density phantom CIRS phantom)		
Modality	CT	CBCT
Company	Philips CT scanner	Versa-High precision (HD) Elekta eXtended Vision Image-guided therapy (XVI) onboard volumetric imaging systemElekta, Crawley, UK)
Voxel size	0.1 × 0.1 × 0.3 cm^3	0.1 × 0.1 × 0.2 cm^3
Dimensions	406 × 406 × 37	500 × 500 × 132
Prime factors values	120 KeV and 213 mA over 470s	120 KeV and 64 mA over 40s
Patient cases		
Modality	CT	CBCT
Company	Philips CT scanner	Versa-High precision (HD) Elekta eXtended Vision Image-guided therapy (XVI) onboard volumetric imaging systemElekta, Crawley, UK)
Voxel size	0.1 × 0.1 × 0.3 cm^3	0.1 × 0.1 × 0.2 cm^3
Dimensions	512×512x168	410×410x84
Prime factors values	120 KeV and 213 mA over 470s	120V and 64 mA over 40s

Legends**:** CIRS**:** Computerized Imaging Reference System, CT: Computed Tomography, CBCT: Cone Beam Computed Tomography, KeV: Kilo-electron volt, mA: Milliampere, cm: Centimetre and UK: Unted Kingdom.

Methodology of default DIR algorithms

In this study, deformable image registration was performed using the open-source toolkit based MATLAB Math Works, Natick) script software tools deformable image registration and adaptive radiotherapy research (DIRART, version 2) and a computational Environment for Rdiological Research (CERR, version 2) in addition to Anatomically Constrained Deformation Algorithm (ANACONDA) available in Raystation treatment planning system [8, 30]. The classes of the four DIRART and CERR algorithms were applying that Optical flow, Demons, Level-set and B-spine algorithm. All experiments were performed on a personal LAPTOP-F2TVIRLR with 8 GB memory, Windows 11 Home system version 24H2) with 3 cores running at 3.3 GHz, utilizing only the CPU, without GPU acceleration.

1- DIR algorithms of DIRART and CERR

The registration process in DIRART used the following steps. Both sets of images were firstly converted from the DICOM format to the CERR format using the CERR software and were then processed. That is, all the pCT and CBCT images were pre-processed before executing the registration. The pre-processing included cropping of the image through removing the treatment table and immobilisation tools using the free, open-source software CERR scripts, leaving only the patient volume in the image, and resizing and resampling the mages to match the size and resolution of CBCT and reduce the computing time. Thus, the pixel volumes of both images were (1, 1, 2) in the direction vector (x, y, z). Whilst the fractional weekly CBCT images are regarded as the reference images and the pCT image is rigidly registered to each CBCT image via the DIRART. The workflow of image registration is shown in Fig. 2. In this study, thirteen intensity-based DIR algorithms were evaluated using an open-source toolkit, called DIRART. These DIR algorithms include iterative optical flow (IOF), Optical Flow (OF), combined Horn–Schunck and Lucas Kanade (CHL), Original Lucas KanadeOLK), HS method with Issam's Non-linear smoothness (HSINS), Improved Lucas Kanade (ILC), Original Schunck Horn Memory saving OSHMS), Modified Demons (MD), Systematic Force Demons (SFD), Double Force Demons (DFD), Original Demons (OD), Fast Demons with Elastic Regularization (FDER), and Free Form (FF). Finally, pCT images were registered to CBCT images using DVF created using algorithms mentioned in last section, yielding dCT via DVF. The mutual information (MI) similarity measure was used in this study.

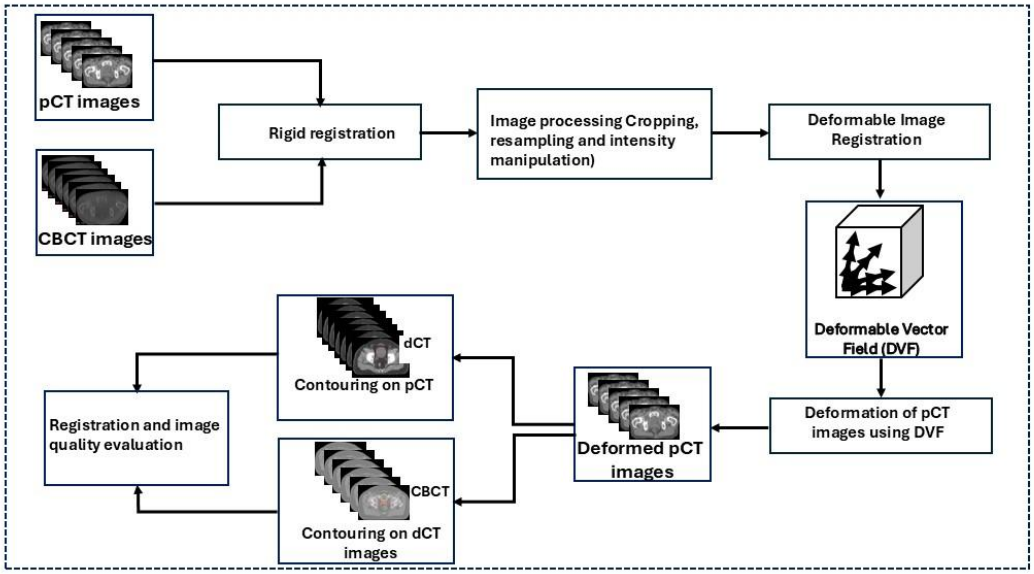


FIG. 2: Workflow for deformable pCT to CBCT images registration as determined by an open-source DIRART and CERR software and Commercial Raystation software.

Legends: pCT: planning Computed Tomography, Cone Beam Computed Tomography, dCT: deformed Computed Tomography and DVF: Deformable Vector Field.

2- DIR algorithms of CERR

Using an open-source DIR tool in CERR, we applied DIR between each patient's pCT and CBCT image. It is possible to configure CERR in single-stage or multistage modes to implement a wide variety of control parameters and registration algorithms. The purpose of this tool is to optimize specific parameters, including subsampling rates and cost function metrics to achieve more accurate registrations. Therefore, a multiresolution method to implement the b-spline deformation algorithm in three stages was applied in this study. To align scans, CERR does not require manual alignment since it has a translation stage that assists in aligning images in the first stage, if required. There are two phases to the DIR registration process. Due to the superior performance of SSD when compared to MI, a similarity measure has been calculated simultaneously with CBCT preprocessing. A spline-based method of registration was developed for CERR, including b-spline and thin-plate splines. DVF was created by applying the b-spline registration method to the CT scans. MATLAB script was used to create dCT images by applying the generated DVF to a pCT image.

3- DIR algorithms of ANACONDA

Better registration accuracy for the local and global image than a regular default step registration was obtained when using ANACONDA registration method. In the Raysearch software, the ANACONDA was verified for the registration of different imaging modalities and also used to propagate contours from pCT to CBCT image in pelvic region using controlled hybrid algorithm [19]. However, the ANACONDA was not verified for scan registration. Therefore, it was adapted in this study and compared with CBCT scan.

Furthermore, Raystation does not directly deform pCT to CBCT. The deformation process in Raystation is achieved by using the script in mhd format and then mhd format is converted to DICOM format using Slicer version 5.2.1). ANACONDA combines anatomical information with image informationHU) which are provided by contoured image sets. The registration process was as following: First**,** after image processing for intensity-based and B-Spline-based registrations mentioned above, both sets of images were converted from the CERR format to the DICOM format using the CERR software as well. Second, both images were uploaded to Raysearch software tool and independently aligned. The MI similarity measure was used in this study. Finally, CT images were registered to CBCT images using DVF created using the uncontrolled and controlled algorithms, yielding dCT via DVF.

Evaluation of registration methods

The accuracy of registration was evaluated using image-quality, registration accuracy and dosimetry verification analysis.

For the phantom, image-quality analysis included signal-to-noise ratio (SNR), contrast-to-noise ratio (CNR), and HU bias as evaluation indices. The HU bias between the reference pCT and CBCT or dCT was calculated as the mean ± standard deviation (SD) and the Identity Function Profile IFP) of the plugs of the CIRS phantom.

CNR was calculated using the following formula:

$$\mathrm{CNR} = \frac{\mathrm{Mean}_{\mathrm{Muscle}} - \mathrm{Mean}_{\mathrm{Adipose}}}{\mathrm{Std}_{\mathrm{Muscle}} + \mathrm{Std}_{\mathrm{Adipose}}} \times 2 \quad \ldots\ldots\ldots\ldots\ldots\ldots\ldots\ldots (1)$$

In the muscle and adipose inserts, $\mathrm{Mean}_{\mathrm{Muscle}}$ and $\mathrm{Mean}_{\mathrm{Adipose}}$ correspond to the means of voxel values, whereas $\mathrm{Std}_{\mathrm{muscle}}$ and $\mathrm{Std}_{\mathrm{Adipose}}$ correspond to the SDs in voxel values. The SNR was calculated by dividing mean by its SD for five ROIs and then calculation the mean SNR. To calculate uniformity, we used the percentage differences between the two mean values.

For the patients, image-quality analysis included the mean absolute error (MAE), the structural similarity index measure (SSIM), and peak signal-to-noise ratio (PSNR). The simulated pCT images were used as reference images.

The MAE can be calculated as follows:

$$\text{MAE} = \frac{\sum_{i=1}^{n} |\text{CT}_{pse}(x_i) - \text{CT}_{ref}(x_i)|}{n} \quad \ldots\ldots\ldots\ldots (2)$$

Where n is the total number of voxelsx_i) at the index position I, CT_{pse} is the dCT, and CT_{ref} is the reference CT image.

The SSIM is defined by the following equation:

$$\text{SSIM}(x,y) = \frac{(2m_x m_y + c_1)(2s_{xy} + c_2)}{(2m_x^2 + m_y^2 + c_1)(2s_x^2 + s_y^2 + c_2)} \quad \ldots\ldots\ldots\ldots\ldots\ldots\ldots\ldots\ldots\ldots (3)$$

Where the average and variance of x are m_x and s_x^2, respectively; the average and variance of y are m_y and s_y^2, respectively; and the covariance of x and y is s_{xy}. C_1 and C_2 are constants calculated as $C1 = k_1 L)^2$ and $C2 = k_2 L)^2$, respectively, where k_1, k_2, and L are 0.01, 0.03, and $2^B - 1$, respectively.

The PSNR is defined by:

$$\text{PSNR} = 10.\log_{10}\left(\frac{\text{MAX}_I^2}{\frac{1}{xy}\sum_{i=0}^{x-1}\sum_{j=0}^{y-1}[I(i,\ j) - K(i,\ j)]^2}\right) \quad \ldots\ldots\ldots\ldots\ldots\ldots\ldots\ldots (4)$$

Where MAX_I is the probable maximum value of an image pixel, and x and y are the image sizes.

Registration accuracy analysis was evaluated as stated by TG-132 by using visual inspection, the Dice similarity coefficient (DSC), and target registration error (TRE) [28]. In the framework of the visual evaluation, the differences between the dCT and CBCT images as well as the checker board images were checked for the phantom and the patients. In DSC, annotations and segmentation outcomes are quantified based on their volumetric overlap. A DSC of 0.0 indicates no overlap, whereas a DSC of 1.0 indicates complete overlap [31]. The DSC is calculated as:

$$\text{DSC} = \frac{2|X \cap Y|}{|X| + |Y|} \quad \ldots\ldots\ldots\ldots\ldots\ldots (5)$$

where |X| and |Y| are the number of elements in the X and Y sets, respectively.

The TRE is the image registration error derived from the difference in position between the corresponding points on the CBCT image and the deformed image. It is calculated as:

$$TRE = \frac{\sum_{j=1}^{n} |x - x'|}{n} \quad \ldots\ldots\ldots\ldots\ldots\ldots\ldots\ldots \quad (6)$$

Where n represents the total number of pairs, and x and x' are the position vectors of the floating and deformed images, respectively.

Data analysis

The correlation of HU values was assessed using the Spearman correlation coefficient. The Kruskal-Wallis H-test was used for performance variations of different DIRs on the same ROI. Whenever the null hypnosis was rejected, a post-hoc test was used to determine a mean that is responsible for rejection of null hypothesis. All statistical analyses were implemented using Microsoft® Excel® 2016 MSOVersion 2211 Build 16.0.15831.20098) 64-bit, and the statistical significance levelthe α-level) used was p = 0.05.

Results

Image quality of phantom study

Fig. 3 illustrates the visual assessment of the DIRART, CERR and Raysearch algorithms to test the best algorithm that can rationally propagate and calculate the intensities and general shapes of the phantom components. All algorithms were able to propagate the HU values from CT to CBCT, but most intensity-based consistent image registration algorithms were unsuccessful in adequately registering CT to CBCT. As shown in Fig. 3, with the exception of IOF, which also failed to satisfactorily register adipose and liver inserts, OF, CHL, OLK, HSINS, ILC, OSHMS, MD, SFD, DFD, OD, FDER, and FF were unable to reproduce the local and global shapes of the phantom components. In addition to IOF, B-Spline algorithm and ANACONDA also performed fairly well in terms of HU values and shapes, matching the globaldisc and head) and localplug) shapes.

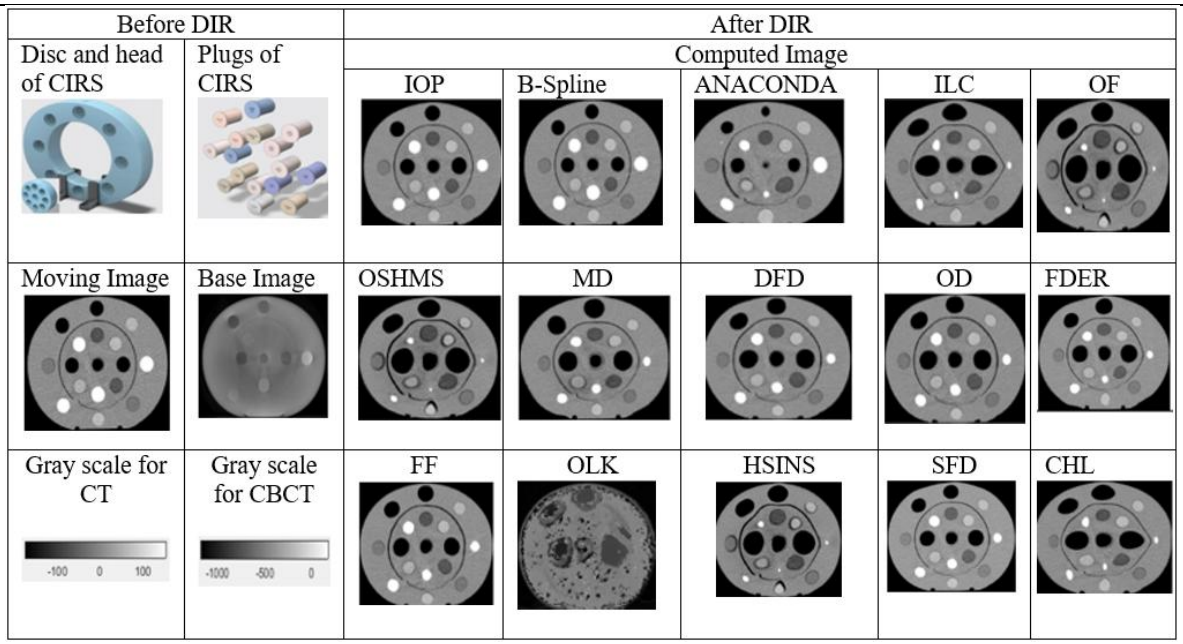
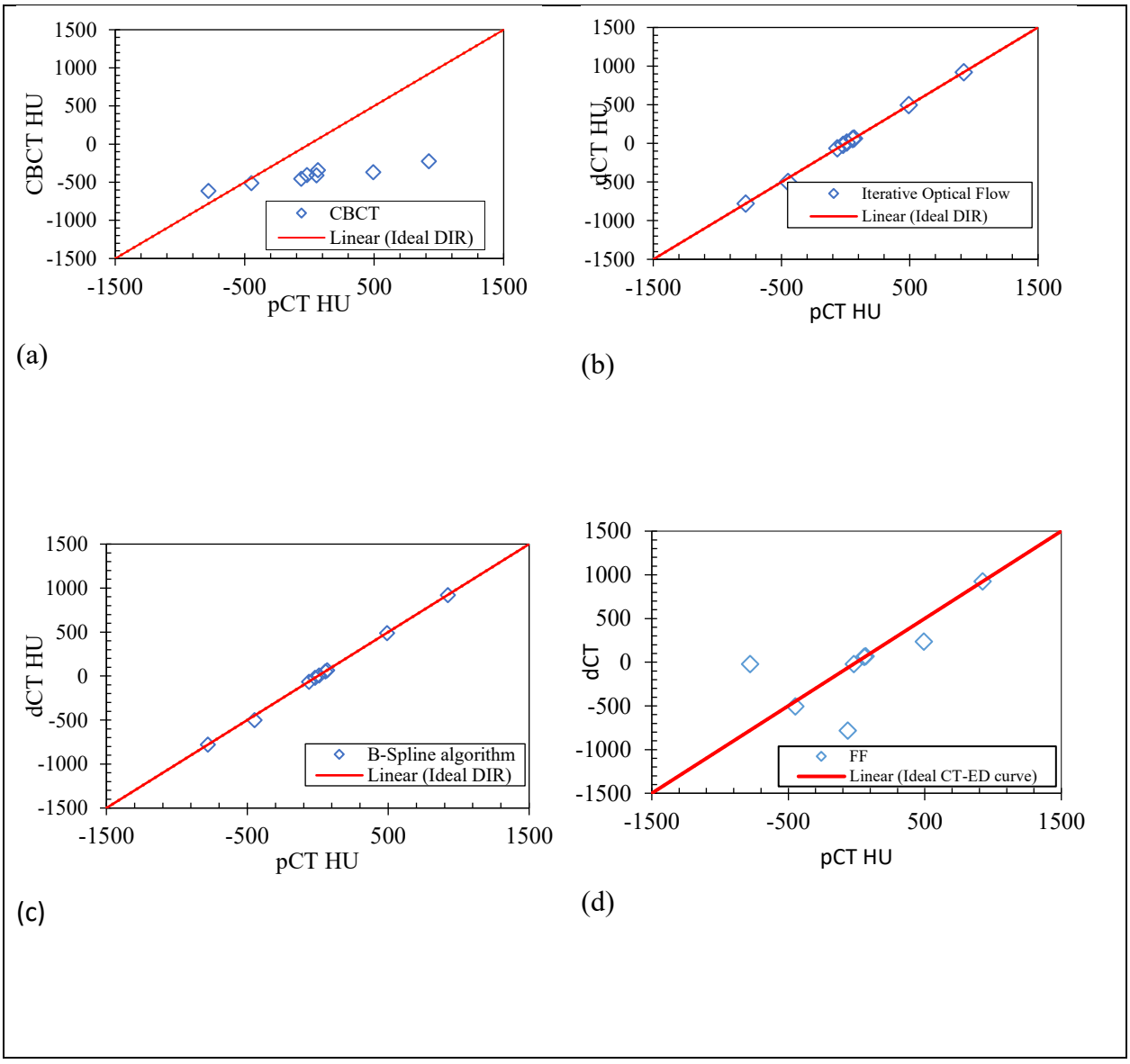


FIG. 3. Assessment of DIR algorithms for the deformation of the phantom. In this stage, CT images are deformed to match CBCT images. The first two columns demonstrate the moving images and base images before registration. The other columns demonstrate each of the deformed images estimated to the base imageCBCT).

Legends: CT: Computed Tomography, CBCT: Cone Beam Computed Tomography, IOF: iterative optical flow, B-S: B-Spline, ANACONDA: Anatomically Constrained Deformation Algorithm, ILC: Improved Lucas Kanade, OF: Optical Flow, OSHMS: Original Schunck Horn Memory saving, MD: Modified Demons, DFD: Double Force Demons, OD: Original Demons, FDER: Fast Demons with Elastic Regularization, FF: Free Form, OLK: Original Lucas Kanade, HSINS : HS method with Issam's Non-linear smoothness, SFD: Systematic Force Demons and CHL: combined Horn–Schunck and Lucas Kanade.

The IFP using CBCT and dCT with IOF and B-Spline, SFD, DFD, FF and ANACONDA algorithms is shown in Fig. 4. As shown in Fig. 4, many subsets of pixels are markedly divergent from the ideal profile, indicating that there are HU values of pixels that are significantly different from the pCT upon application of the original CBCT. On the other hand, the consistency of the pixel intensity improved significantly with the application of DIR. For instance, the percentage

difference ranged from 13.48% to 99% for CBCT, while with DIR, the differences were within 26.82%) for all plugs when using IOF, B-Spline and ANACONDA.


1500
1000
500
0
-500
-1000
-1500
CBCT HU
-1500
-500
500
1500
pCT HU
CBCT
Linear (Ideal DIR)
(a)
dCT HU
Iterative Optical Flow
Linear (Ideal DIR)
(b)
B-Spline algorithm
Linear (Ideal DIR)
(c)
dCT
FF
Linear (Ideal CT-ED curve)
(d)

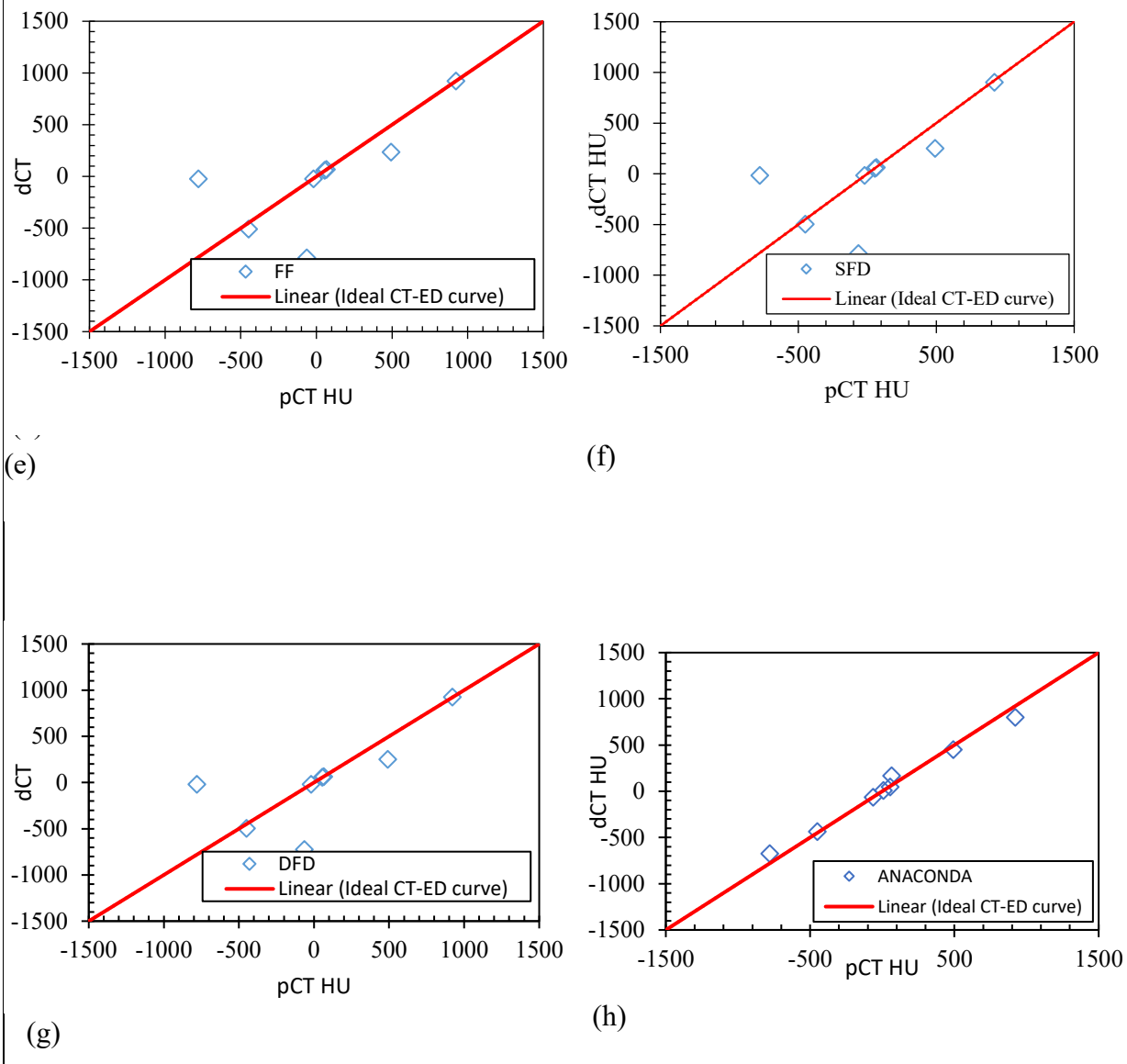


FIG. 4. Correlation of HU values between pCT and CBCT scansa) and dCTa, b, c, d, e, f, g and h). HU correlations were plotted for CBCT without correction and dCTIOF),B-Spline),SFD),DFD), FF) and ANACONDA).

Legend CBCT: Cone Beam Computed Tomography, pCT: planning Computed Tomography, dCT: deformed Computed Tomography, FF: Free Form, SFD: Systematic Force Demons, DFD: Double Force Demons, ANACONDA: Anatomically Constrained Deformation Algorithm and HU: Hounsfield Unit.

Table 2 contains the image quality indices derived for the five CT modalities: pCT, CBCT, IOF-based dCT, B-Spline-based dCT, combined-based CT and ANACONDA-based dCT. In all three metrics, uniformity, CNR, and SNR, CBCT performed worse than the other metrics. The dCT generated by the proposed different types of DIR methods showed noticeable enhancement in uniformityrelative decreases of 75%), 65%), 75%) and 77%), CNRrelative increases of 214%), 213%), 215%) and 216%, and SNRrelative increases of 108%),107%), and 107% for IOF, B-Spline, and steps relative to those of CBCT, respectively. DIR-based dCT also showed good improvement over CBCT in terms of image quality.

TABLE 2 demonstration of the results of the CIRS phantom for image quality.

Index	pCT	CBCT	IOF	B-Spline	ANACONDA
Uniformity	1.000%	2.000%	0.500%	0.700%	0.460%
CNR	9.480	-8.150	9.300	9.250	9.440
SNR	3.500	-78.560	6.330	5.880	5.870

Legend: CIRS: Computerized Imaging Reference System, pCT: planning Computed Tomography, CBCT: Cone Beam Computed Tomography, IOP: Iterative Optical Flow, ANACONDA: Anatomically Constrained Deformation Algorithm and SNR: Signal-to-Noise ratio CNR: Contrast-to-Noise ratio.

Image quality and registration performance of patient cases of the patient study

Fig. 5 tests on whether algorithms of the DIRART, CERR and Raysearch software items can rationally calculate and propagate the HU and global in addition to local shapes of the pelvic structures in prostate cancer cases. Based on visual check using checkerboard images of visualization options in the DIR softwarebefore and after registration), although all algorithms were able to propagate the HU values from CT to CBCT, all default registration algorithms were unsuccessful in adequately registering CT to CBCT. In contrast, the ANACONDA registration methods succussed in registering pCT to CBCT in terms of HU values and shapes, matching the globalbody) and localtarget and organs at risk) shapes. This is because when optical flow is combined with override, theoretical condition of optical flow, which states that the intensity of objects in successive images must remain constant, is followed [32].

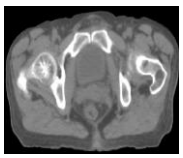
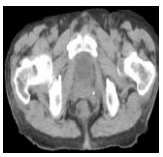
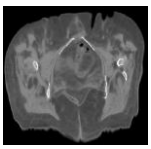
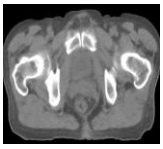
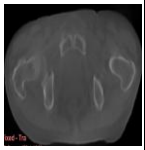
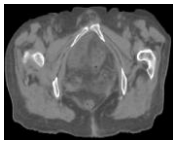
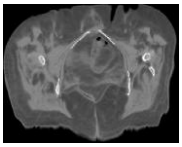
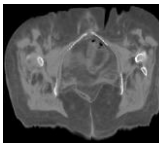
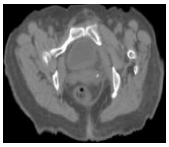
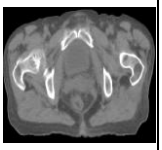
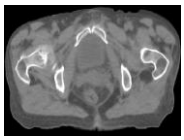
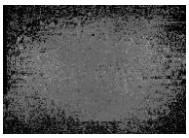
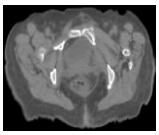
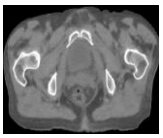
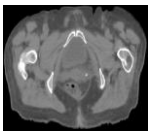
Before DIR		After DIR				
Male pelvis		Computed image				
		IOF	B-Spline	FF	ANACONDA	HSINS
						
Moving imageCT)	Base ImageCBCT)	ILC	OF	OSHMS	MD	SFD
						
Gray scale (HU) for CT	Gray scale (HU) for CBCT	DFD	OLK	FDER	OD	CHL
						

FIG. 5. Quality evaluation of deformable registration for the prostate cancer cases. CT images and CBCT images were registered to create dCT images.

Legend: CT: Computed Tomography, CBCT: Cone Beam Computed Tomography, IOF: iterative optical flow, B-S: B-Spline, FF: Free Form, ANACONDA: Anatomically Constrained Deformation Algorithm, HSINS : HS method with Issam's Non-linear smoothness, ILC: Improved Lucas Kanade, OF: Optical Flow, OSHMS: Original Schunck Horn Memory saving, MD: Modified Demons, SFD: Systematic Force Demons, DFD: Double Force Demons, , OLK: Original Lucas Kanade, FDER: Fast Demons with Elastic Regularization, OD: Original Demons and CHL: combined Horn–Schunck and Lucas Kanade.

A comparison of the average outcomes of quantitative image quality for the eight CT modalities based on patient data is presented in Table 3. As can be seen in Table 3, the DIR methods outperformed all evaluation indices. Compared with the original CBCT, the dCTs generated by IOF, B-Spline, the SFD, DFD FF and ANACONDA all improved significantly. SSIM values were improved by 14%), 9%), 9%), 11%), 21%), 23%) and 14%) for seven DIR methods relative to, PSNR improved by 98%), 87%), 87%), 76%), 97%), 94%) and 93%), respectively. The MAE range improved from 331.14 for CBCT to 7.9, 41.45, 43.45, 80.53, 8.3, 21.15 and 23 for IOF, SFD, DFD FF B-Spline and ANACONDA respectively. Furthermore, according to Table 3, the prostate cancer cases were matched by landmarks. In comparison to IOF and B-Spline, SFD, DFD and FF-based methods, the error magnitude of average registration was reduced by approximately 67%)from about 0.7 cm to 0.2 cm) for ANACONDA registration methods.

TABLE 3. Results of the patient image quality and mean and standard deviation of TRE for landmarks in five prostate tumours, except registration error of CBCT, which is not applicable since CBCT was used as the reference. For the five cases of prostate cancer, all landmarks were used to calculate the absolute error values.

Modality	**SSIM**	**PSNR (dB)**	**MAE HU**	**Correlation Coefficient**	**Target Registration Error (cm)**
CBCT	0.94±0.020	45.17±1.330	331.140	0.38±0.032	not applicable
IOF	0.99±0.004	51.71±0.640	7.900	0.70±0.065	0.700 ± 0.600
SFD	0.97±0.020	49.23±2.110	41.450	0.66±0.061	0.650 ± 0.220
DFD	0.97±0.020	49.46±1.810	43.450	0.64±0.060	0.600 ± 0.400
FF	0.97±0.020	50.15±2.230	80.530	0.69±0.064	0.680 ± 0.510
B-Spline	0.99±0.003	54.79±4.360	8.300	0.51±0.047	0.690 ± 0.350
ANACONDA	0.98±0.004	51.50±3.230	23.000	0.93±0.087	0.222 ± 0.130

* Legend: SSIM: Structural Similarity Index measure, PSNR (dB): peak signal-to-noise ratio, MAE: the Mean Absolute Error.

The results of the critical organ and target volume matching are summarized in Table 4. This includes the DSC metric calculated for the treatment target and critical organs for sole deformable registration IOF, B-Spline, SFD, DFD, FF, registration), ANOCANDA No-controlling structures and ANOCANDA Controlling structures**)**. The results indicated that ANACONDA significantly improved volume matching. Improvements of about 49.5%) and 46.4%) were observed in the average DSC value when comparing the ANACONDA to other deformable registrations. As indicated by Brock et al., adequate volume matching for adaptive radiotherapy applications should be 80%) or higher. As shown in Table 4, the results of the ANACONDA were suitable for ART [33]. Quantitatively, this method improves scan matching of overall image, treatment target and the critical at-risk organs by about override ratio of 60%) in comparison to other methods. Therefore, override ratio becomes more than 90%) for critical structures. It is evident that the overall image and treatment target in addition to the critical at-risk organs are mostly registered well with ANACONDA registration. Generally, with this method, the results of volume matching are considerably enhanced.

TABLE 4. Average DSC for sole registration methods of five patients.

Organ	Bladder	Rectum	Treatment target
IOF-based registration	0.516±0.090	0.63±0.080	0.602±0.170
B-Spline-based registration	0.53±0.100	0.66±0.070	0.606±0.170
SFD-based registration	0.56±0.130	0.64±0.051	0.67±0.166
DFD-based registration	0.60±0.139	0.65±0.064	0.68±0.162
FF-based registration	0.56±0.157	0.66±0.043	0.65±0.158
ANOCANDANo-controlling structures)	0.56±0.157	0.66±0.043	0.65±0.158
ANOCANDAControlling structures)	0.94±0.020	0.87±0.040	0.91±0.030

Legend: IOF: Iterative Optical Flow, SFD: Systematic Force Demons, DFD: Double Force Demons, FF: Free Form and ANACONDA: Anatomically Constrained Deformation Algorithm.

Table 5 shows that comparisons among sole registration methods in addition to ANACONDA method in terms of DSC using Kruskal-Wallis H-test and post-hoc test. Differences were significant in the median rating of the DSC values by the seven groupsIOF, B-Spline, SFD, DFD and FF, ANOCANDANo-controlling structures) and ANOCANDAcontrolling structures)) as examined by the Kruskal-Wallis H-test at the α-Level ≤ 0.05. Therefore, the null hypothesis was rejected. Null hypothesis refers to the absence of systematic error in the analytical method. The term null means the observed and reference values are identical disregarding that owning to random variation. When the probability that chance falls lead to the observed difference, the null hypothesis is highly unlikely true null hypothesis is rejected). On the other hand, when the probability that there is no difference between the observed and reference values, the null hypothesis is highly likely true null hypothesis failed to reject) [34, 35]. Further test with Dunn's Q post-hoc test demonstrated that the CBCT and controlling structures) ANACONDA valued the DSC significantly better than did the IOF, B-Spline, SFD, DFD, FF or non-controlling structures) and that difference was not significant in the scores between the CBCT and ANACONDA for bladder, target and rectum. It could therefore be inferred that sole algorithms failed to register the pCT to CBCT correctly and they were similar in their performance since the H-values were below 5.99 at p value ≤ 0.05 and the H-values were over 5.99 at p value ≤ 0.05 when ANACONDA

method and CBCT were added to them. Furthermore, ANACONDA method succeeded to register the pCT to CBCT correctly since the H-values were below 5.99 at p value ≤ 0.05.

Table5): Kruskal-Wallis H-test with post-hoc test. The critical value for the f-test at the α-Level ≤ 0.05 is 5.99 obtained from the chi-square table.

	Sole algorithms			Sole algorithms in addition to ANACONDA and CBCT method			ANACONDA controlling structures) and CBCT method		
Critical organs	H-Value	P-Value	Null hypothesis	H-Value	P-Value	Null hypothesis	H-Value	P-Value	Null hypothesis
Bladder	1.55	0.46	Fail to Reject	13.18	0.0014	Reject Null	4.81	0.09	Fail to Reject
Rectum	1.78	0.41	Fail to Reject	13.34	0.0013	Reject Null	0.10	0.95	Fail to Reject
Target	0.88	0.65	Fail to Reject	13.34	0.0013	Reject Null	3.15	0.21	Fail to Reject

***** Legend: H-value: Kruskal-Wallis H-test with post-hoc test; P-Value, CBCT: Cone Bean Computed Tomography and ANACONDA: Anatomically Constrained Deformation Algorithm.

Discussion

In this study, the ability of fifteen DIR algorithms to propagate scan from pCT to CBCT images was extensively evaluated. Four registration methods, IOF, B-Spline and ANACONDA registration methods, succeeded in reproducing pCT HU values based on visual and quantitative evaluation. Figure 3, Figure 4 and Table 2), thereby decreasing uniformity of 75%), 65%),75%), 77% and improving both CNRof 214%), 213%), 215%), 216%, and SNRof 108%), 107%),107%), 107% relative to those of CBCT for phantom. As demonstrated in this study, all four registration methods were quantitatively efficient in propagating HU values such that the HU accuracy in dCT was comparable to that in pCT images indicating that the type of registration method played a minor role in modifying the pCT in terms of HU value propagation.

Compared to CBCT images, SSIM, PSNR, and MAE in patients in the results of the dCT images, Table 3 showed a significant improvement in the HU value. There were enhancements in SSIM of (5%, 3%, 3%, 3%, 5% and 4%), PSNR of (14%, 21%, 9%, 9%, 11% and 24%), and MAE

of (98%, 97%, 87%, 87%, 76% and 93%) relative to those of CBCT for patients with the IOF, B-Spline, SFD, DFD, FF and ANACONDA registration methods, respectively.

Most studies have succeeded in calculating transformations and propagating the contour from pCT to CBCT using DVF with B-Spline algorithms [19, 36-37]. Thus, they reported good geometric agreement for the atypical anatomy of the pelvis encountered in the clinic. Interestingly, in contrast to these experimental findings, it was found that intensity-based registration and point-based registration completely failed to sufficiently register both the global and local shapes of the pelvis without modifying the registration methods, yet the ANACONDA registration methods improved registration accuracy and the registration accuracy was comparable to the results of Yang et al. as in Table 4 [30].

Finite element models (FEMs)-based deformable registration algorithm is used in Hybrid DIR as a first condition using anatomical information, for instance the manual contouring on the pCT and CBCT and intensity-based algorithm is used as a second condition using the image intensity information. The evaluation is based on DSC that quantities the overlapping volume amount, and TRE that can only estimate the displacement between two structures; however, the spatial accuracy, including registration of the image within and outside the structure, is ignored in this assessment. Therefore, the spatial accuracy might be low for intensity, B-Spline and hybrid algorithms. The DSCs for the critical target, bladder and rectum using ANACONDA registration process were ≥ 0.9, which is comparable with the outcome of other study for intensity-based two-step registration process [38]. In this registration process, the target and source images are contoured, registration is then performed using FEMs registration and the displacement vector fields from first registration is finally used to deform the floating images. Hybrid method and intensity based two-step registration process are basically different, and they are associated with advantages and disadvantages. An important aspect is that ANACONDA registration process matches both structure contours and image intensity after contouring without the intensity manipulation process converting the structure contours into further image intensity data. Therefore, the ANACONDA registration process could generate more accurate voxel mapping inside and outside the critical structures due to better utility of image intensity information and takes less time, but spatial accuracy has not been assessed yet. Therefore, further studies that compares ANACONDA with the intensity-based two-step registration and B-spline-based two-

step registration processes are required so as to clarify the spatial DIR accuracy for these registration processes [38-39].

As shown in Table 4. This might be due to the fact that DIRs are more prone to error in low-contrast regions. Hence, failure of DIR in specifying sufficient contrast edges might occur, which prevents DIRs from correctly deriving intensity-based DIRs [18]. It succeeded in producing TRE and DSC comparable to cases with the same modality registration, within 0.3 cm TRE and $\geq$ 0.8 DSC in the pelvis, consistent with suggestions of other publications [29, 40-42]. Furthermore, one aspect of the B-Spline algorithm is that it works well for images that are feature-rich with little or no ambiguity between the matching points in moving and base images. However, CBCT images have limitations that prevent successful registration between pCT and CBCT in addition to poor application of the algorithm or model limitations intrinsic to the algorithm. For instance, transmitted projections with high scatter photons in CBCT degrades the image quality, and prevents the algorithm of energy-minimizing splinessnakes) from measuring local variations in image valuesgradient ∇) accurately [43-46].

Conclusion

Despite the fact that the B-Spline and IOF algorithms succeeded in satisfactorily registering the CIRS phantom, they failed to reproduce the geometry of prostate patient cases. Thus, to reproduce the geometry of the pelvis, further supplementary information of the organ is required to create an accurate DVF for the treatment target and critical structures, especially by combining the intensity override with the OF registration method or finite element models hybridized with intensity-based algorithm, as shown in the ANACONDA registration methods.

Ethical approval

This work was approved by ethical committee of the university with this code: IR.TUMS.IKHC.REC.1400.290

Informed consent

I understand that my participation in this study is voluntary and that I may choose to withdraw any time. I freely agree to participate in this research study. I understand that all efforts will be made to keep information regarding my personal identity confidential.

Conflict of Interest

Statement “The authors have no conflicts of interest to declare.”

References

[1] Bourland JD, editor. Image-guided radiation therapy. Crc Press; 2012 Feb 22. https://doi.org/**10.1201/b11627**

[2] Khan FM, Gibbons JP. Khan's the physics of radiation therapy. Lippincott Williams & Wilkins; 2014.

[3] Kirby M, Calder KA. On-treatment verification imaging: a study guide for IGRT. CRC Press; 2019 Apr 15.

[4] Yan D, Vicini F, Wong J, Martinez A. Adaptive radiation therapy. Physics in Medicine & Biology. 1997;42(1):123. https://doi.org/10.1088/0031-9155/42/1/008

[5] Anaya VM, Fairfoul J. Assessing the feasibility of adaptive planning for prostate radiotherapy using Smartadapt deformable image registration. Medical Engineering & Physics. 2019;64:65-73. https://doi.org/10.1016/j.medengphy.2019.01.001

[6] Michalski JM, Yan Y, Watkins-Bruner D, Bosch WR, Winter K, Galvin JM, Bahary JP, Morton GC, Parliament MB, Sandler HM. Preliminary toxicity analysis of 3-dimensional conformal radiation therapy versus intensity modulated radiation therapy on the high-dose arm of the Radiation Therapy Oncology Group 0126 prostate cancer trial. International Journal of Radiation Oncology* Biology* Physics. 2013 Dec 1;87(5):932-8. https://doi.org/10.1016/j.ijrobp.2013.07.041

[7] De Crevoisier R, Bayar MA, Pommier P, Muracciole X, Pêne F, Dudouet P, Latorzeff I, Beckendorf V, Bachaud JM, Laplanche A, Supiot S. Daily versus weekly prostate cancer image guided radiation therapy: phase 3 multicenter randomized trial. International Journal of Radiation Oncology* Biology* Physics. 2018 Dec 1;102(5):1420-9.. https://doi.org/10.1016/j.ijrobp.2018.07.2006

[8] Deasy JO, Blanco AI, Clark VH. CERR: a computational environment for radiotherapy research. Medical physics. 2003;30(5):979-85. https://doi.org/10.1118/1.1568978

[9] Roeske JC, Forman JD, Mesina CF, He T, Pelizzari CA, Fontenla E, Vijayakumar S, Chen GT. Evaluation of changes in the size and location of the prostate, seminal vesicles, bladder, and rectum during a course of external beam radiation therapy. International journal of radiation oncology, biology, physics. 1995 Dec 1;33(5):1321-9. https://doi: 10.1016/0360-3016(95)00225-1

[10] Lemus OM, Tanny S, Cummings M, Webster M, Wancura J, Jung H, Zhou Y, Yoon J,

Pacella M, Zheng D. Influence of air mapping errors on the dosimetric accuracy of prostate CBCT-guided online adaptive radiation therapy. Journal of Applied Clinical Medical Physics. 2023 Oct;24(10):e14057. https://doi.org/10.1002/acm2.14057

[11] Mundt AJ, Roeske JC, editors. Image-guided radiation therapy: a clinical perspective. PMPH-USA; 2010 Dec 31.

[12] Onozato Y, Kadoya N, Fujita Y, Arai K, Dobashi S, Takeda K, Kishi K, Umezawa R, Matsushita H, Jingu K. Evaluation of on-board kV cone beam computed tomography–based dose calculation with deformable image registration using Hounsfield unit modifications. International Journal of Radiation Oncology* Biology* Physics. 2014;89(2):416-23. https://doi.org/10.1016/j.ijrobp.2014.02.007

[13] Giacometti V, Hounsell AR, McGarry CK. A review of dose calculation approaches with cone beam CT in photon and proton therapy. Physica Medica. 2020 Aug 1;76:243-76. https://doi.org/10.1016/j.ejmp.2020.06.017

[14] Fotina I, Hopfgartner J, Stock M, Steininger T, Lütgendorf-Caucig C, Georg D. Feasibility of CBCT-based dose calculation: comparative analysis of HU adjustment techniques. Radiotherapy and Oncology. 2012 Aug 1;104(2):249-56. https://doi.org/10.1016/j.radonc.2012.06.007

[15] Jassim H, Nedaei HA, Geraily G, Banaee N, Kazemian A. The geometric and dosimetric accuracy of kilovoltage cone beam computed tomography images for adaptive treatment: a systematic review. BJR| Open. 2023 Nov 1;5(1):20220062. https://doi.org/10.1016/j.radonc.2009.07.012

[16] Jassim HH, Nedaei HA, Banaee N, Geraily G, Kazemian A. An Investigation of Dosimetric Consequences of the Anatomic Changes at First Fraction in VMAT of Prostate Cancer Cases using Deformable Planning CT and KVCBCT Image Registration. Journal of Biomedical Physics and Engineering. 2023 Sep 11. https://doi:10.31661/jbpe.v0i0.2212-1574.

[17] Moteabbed M, Sharp GC, Wang Y, Trofimov A, Efstathiou JA, Lu HM. Validation of a deformable image registration technique for cone beam CT-based dose verification. Medical physics. 2015;42(1):196-205. https://doi.org/10.1118/1.4903292

[18] Yang Y, Schreibmann E, Li T, Wang C, Xing L. Evaluation of on-board kV cone beam CTCBCT)-based dose calculation. Physics in Medicine & Biology. 2007 Jan 12;52(3):685. https://doi.org/10.1088/0031-9155/52/3/011

[19] Woerner AJ, Choi M, Harkenrider MM, Roeske JC, Surucu M. Evaluation of deformable image registration-based contour propagation from planning CT to cone-beam CT. Technology in cancer research & treatment. 2017;16(6):801-10. https://doi.org/10.1177/1533034617697242

[20] Varadhan R, Karangelis G, Krishnan K, Hui S. A framework for deformable image registration validation in radiotherapy clinical applications. Journal of applied clinical medical physics. 2013 Jan;14(1):192-213. https://doi.org/10.1120/jacmp.v14i1.4066.

[21] Shah KD, Shackleford JA, Kandasamy N, Sharp GC. Improving deformable image registration accuracy using a hybrid similarity metric for adaptive radiation therapy. InMedical Imaging 2021: Image Processing 2021 Feb 15Vol. 11596, pp. 944-950). SPIE.

[22] Imae T, Haga A, Watanabe Y, Takenaka S, Shiraki T, Nawa K, Ogita M, Takahashi W, Yamashita H, Nakagawa K, Abe O. Retrospective dose reconstruction of prostate stereotactic body radiotherapy using cone-beam CT and a log file during VMAT delivery with flattening-filter-free mode. Radiological Physics and Technology. 2020 Sep;**13**(3):238-48. https://doi.org/10.1007/s12194-020-00574-3

[23] Xie L, He K, Gong J, Xu D. Multi-Intensity Optimization-Based CT and Cone Beam CT Image Registration. Electronics. 2022;11(12):1862. https://doi.org/10.3390/electronics11121862

[24] Giacometti V, King RB, Agnew CE, Irvine DM, Jain S, Hounsell AR, McGarry CK. An evaluation of techniques for dose calculation on cone beam computed tomography. The British journal of radiology. 2019;92(1096):20180383. https://doi.org/10.1259/bjr.20180383

[25] Marchant TE, Joshi KD, Moore CJ. Accuracy of radiotherapy dose calculations based on cone-beam CT: comparison of deformable registration and image correction based methods. Physics in Medicine & Biology. 2018 Mar 12;63(6):065003. https://doi.org/ 10.1088/1361-6560/aab0f0

[26] Fotina I, Hopfgartner J, Stock M, Steininger T, Lütgendorf-Caucig C, Georg D. Feasibility of CBCT-based dose calculation: comparative analysis of HU adjustment techniques. Radiotherapy and Oncology. 2012 Aug 1;104(2):249-56. https://doi.org/10.1016/j.radonc.2012.06.007

[27] Giacometti V, King RB, Agnew CE, Irvine DM, Jain S, Hounsell AR, McGarry CK. An evaluation of techniques for dose calculation on cone beam computed tomography. The British journal of radiology. 2019;92(1096):20180383. https://doi.org/10.1259/bjr.20180383

[28] Density E. Image Quality Phantom System. Product Guide.

[29] Brock KK, Mutic S, McNutt TR, Li H, Kessler ML. Use of image registration and fusion algorithms and techniques in radiotherapy: Report of the AAPM Radiation Therapy Committee Task Group No. 132. Medical physics. 2017 Jul;44(7):e43-76. https://doi.org/10.1002/mp.12256

[30] Yang D, Brame S, El Naqa I, Aditya A, Wu Y, Murty Goddu S, Mutic S, Deasy JO, Low DA. DIRART–A software suite for deformable image registration and adaptive radiotherapy research. Medical physics. 2011;38(1):67-77. https://doi.org/10.1118/1.3521468

[31] Dice LR. Measures of the amount of ecologic association between species. Ecology. 1945 Jul 1;26(3):297-302. https://doi.org/10.2307/1932409

[32] Barron JL, Fleet DJ, Beauchemin SS. Performance of optical flow techniques. International journal of computer vision. 1994;12(1):43-77. https://doi.org/10.1007/BF01420984

[33] Brock KK, Mutic S, McNutt TR, Li H, Kessler ML. Use of image registration and fusion algorithms and techniques in radiotherapy: Report of the AAPM Radiation Therapy Committee Task Group No. 132. Medical physics. 2017 Jul;44(7):e43-76. https://doi.org/10.1002/mp.12256

[34] Plichta SB, Garzon LS. Statistics for nursing and allied health. Lippincott Williams & Wilkins; 2009.

[35] Miller J, Miller JC. Statistics and chemometrics for analytical chemistry. Pearson education; 2018 Apr 26.

[36] Chao M, Xie Y, Xing L. Auto-propagation of contours for adaptive prostate radiation therapy. Physics in Medicine & Biology. 2008 Aug 1;53(17):4533. https://doi.org/10.1088/0031-9155/53/17/005

[37] Li X, Zhang Y, Shi Y, Wu S, Xiao Y, Gu X, Zhen X, Zhou L. Comprehensive evaluation of ten deformable image registration algorithms for contour propagation between CT and cone-beam CT images in adaptive head & neck radiotherapy. PloS one. 2017;12(4):e0175906. https://doi.org/10.1371/journal.pone.0175906

[38] Jassim H, Nedaei HA, Geraily G, Banaee N, Kazemian A, Seifi MD. Evaluation of Geometric and Dosimetric Accuracy of Deformable Image Registration of Target and Critical Organs in Prostate CBCT-Guided Adaptive Radiotherapy. Journal of Applied Clinical Medical Physics. 2024. https://doi:10.1002/acm2.14490.

[39] Takayama Y, Kadoya N, Yamamoto T, Ito K, Chiba M, Fujiwara K, Miyasaka Y, Dobashi S, Sato K, Takeda K, Jingu K. Evaluation of the performance of deformable image registration between planning CT and CBCT images for the pelvic region: comparison between hybrid and

intensity-based DIR. Journal of radiation research. 2017 Jul 1;58(4):567-71. https://doi.org/10.1093/jrr/rrw123

[40] Shekhar R, Lei P, Castro-Pareja CR, Plishker WL, D'Souza WD. Automatic segmentation of phase-correlated CT scans through nonrigid image registration using geometrically regularized free-form deformation. Medical physics. 2007;34(7):3054-66. https://doi.org/10.1118/1.2740467

[41] Zhang T, Chi Y, Meldolesi E, Yan D. Automatic delineation of on-line head-and-neck computed tomography images: toward on-line adaptive radiotherapy. International Journal of Radiation Oncology* Biology* Physics. 2007;68(2):522-30. https://doi.org/10.1016/j.ijrobp.2007.01.038

[42] Goldberg-Zimring D, Talos IF, Bhagwat JG, Haker SJ, Black PM, Zou KH. Statistical validation of brain tumor shape approximation via spherical harmonics for image-guided neurosurgery. Academic radiology. 2005 Apr 1;12(4):459-66. https://doi.org/10.1016/j.acra.2004.11.032

[43] Lee S, Wolberg G, Chwa KY, Shin SY. Image metamorphosis with scattered feature constraints. IEEE transactions on visualization and computer graphics. 1996 Dec;2(4):337-54. https://doi.org/10.1109/2945.556502

[44] Yang D, Chaudhari SR, Goddu SM, Pratt D, Khullar D, Deasy JO, El Naqa I. Deformable registration of abdominal kilovoltage treatment planning CT and tomotherapy daily megavoltage CT for treatment adaptation. Medical physics. 2009;36(2):329-38. https://doi.org/10.1118/1.3049594

[45] Yeo UJ, Supple JR, Taylor ML, Smith R, Kron T, Franich RD. Performance of 12 DIR algorithms in low-contrast regions for mass and density conserving deformation. Medical physics. 2013;40(10):101701. https://doi.org/10.1118/1.4819945

[46] Hajnal JV, Hill DL. Medical image registration. CRC press; 2001. 392 p.